CANN, C. and SAHARUDIN, M.S. 2023. Design and fabrication of a wrist splint for burn patient rehabilitation using 3D printing technologies. *Journal of physics: conference series* [online], 2643: proceedings of the 8th International conference on applications and design in mechanical engineering 2023 (ICADME 2023), 4-5 September 2023, Kuala Lumpur, Malaysia, article 012003. Available from: https://doi.org/10.1088/1742-6596/2643/1/012003

Design and fabrication of a wrist splint for burn patient rehabilitation using 3D printing technologies.

CANN, C. and SAHARUDIN, M.S.

2023

Design and fabrication of a wrist splint for burn patient rehabilitation using 3D printing technologies.

Connor Cann and Mohd Shahneel Saharudin

School of Engineering, Robert Gordon University, Garthdee Road, AB10 7QB, Aberdeen, UK.

s.saharudin@rgu.ac.uk

Abstract. Severe and common injuries involving burns to the hands and wrists can often lead to permanent loss of motion. The issue is exacerbated by the delicate nature of tendons and muscles in the hands, along with the formation of scar tissue. While rehabilitation exercises can help improve the range of motion, early-stage recovery requires additional tension on the affected areas. To address this concern, a novel project was initiated, aiming to develop a specialized splint for later-stage rehabilitation. This innovative splint allows users to carry out their daily tasks while wearing it, constantly applying a beneficial load on the wrist, hand, and digits to enhance range of motion. The development of the splint involved leveraging Fused Deposition Modelling (FDM) 3D printing and medically safe materials for the initial prototype. Finite Element Analysis (FEA) was employed to analyze the design. The process underwent iterative design improvements and parameter adjustments, ultimately resulting in the final prototype. The FEA analysis confirmed the strength and durability of the PLA components, while the TPU digit resistance bands were evaluated using a hyper-elastic model. As a result, the final design effectively applies tension to the digits without compromising day-to-day tasks' usability and wearer's comfort. Future iterations of the splint could focus on enhancing fastening methods, reducing brace movement during usage, creating various sizes to accommodate different arm/hand dimensions, and optimizing mass-manufacturing processes.

1. Introduction

Hand and wrist burns are both prevalent and severe among burn patients [1]. Research indicates that a considerable number of burn patients necessitate surgical interventions, ranging from skin grafts to amputation. Notably, reduced range of motion (ROM) is observed in the hands and wrists of burn patients [2–4]. Several factors contribute to this reduction, including damage to tendons and joints, the formation of scar tissue, and scar tissue contracture, which can vary based on the extent of the burn injury [5]. Burns can cause significant damage to joints and tendons due to their superficial nature, leading to a prompt reduction in range of motion (ROM) shortly after the burn incident. Subsequently, scarring becomes apparent on the hand, and this can result in substantial scar contracture [6]. In later stages, ROM reduction is predominantly caused by scar contracture [7]. Furthermore, research indicates that even after a 12-month period, the wrists exhibit considerable reduction in ROM, showing minimal improvement from the initial ROM after the burn event, mainly due to the impact of scar contracture [8]. The extension of the wrists experienced a notable reduction in range of motion (ROM) within a 12-month period [9]. Therefore, the main emphasis of rehabilitation endeavors lies in preventing the loss of ROM in extension [9,10].

There are three distinct degrees of burn severity that can be identified and described: superficial, superficial/deep partial, and complete thickness [11]. Range of motion (ROM) in the long run is unaffected by superficial burns because they only damage the top dermal layer, causing mild redness and pain without harming underlying muscles and tendons [12]. Superficial/deep partial burns involve some or all of the dermis layer and cause redness, blistering, discomfort, and swelling that might temporarily restrict motion but usually do not affect mobility. Full-thickness burns cause significant tissue loss, blackened flesh, swelling, and occasionally loss of feeling since they impact all layers of skin and often underlying tissues and bone. Patients who suffer from severe burns often need to undergo surgery and grafting, which can cause permanent damage to their range of motion (ROM). This study aims to address this issue by using FDM printing [13] to make a durable and comfortable wrist brace for the purpose of extending the tendons of severely burned patients during rehabilitation in order to increase their range of motion (ROM) [2,14]. Most importantly, this layout keeps the patient's functional use of their hand unaffected by the healing and rehabilitative processes [15,16].

2. Materials and method

The design parameters in figure 1 were established based on a comprehensive literature review, focusing on enhancing the ROM rehabilitation process using FDM printed components while minimizing non-FDM printed parts, prioritizing medical safety, wearer comfort, and modularity of the wearable device, ensuring no irritation, discomfort, or damage to injured tissue, guaranteeing comfort on the skin and unrestricted hand/wrist movement, considering secondary aspects such as durability, simplicity, adjustability, and user-friendliness for patients and doctors. Besides that, tertiary concerns like a lightweight, thin, and compact design that can be discreetly worn under or over garments, while maintaining an ergonomic and appealing aesthetic [17].

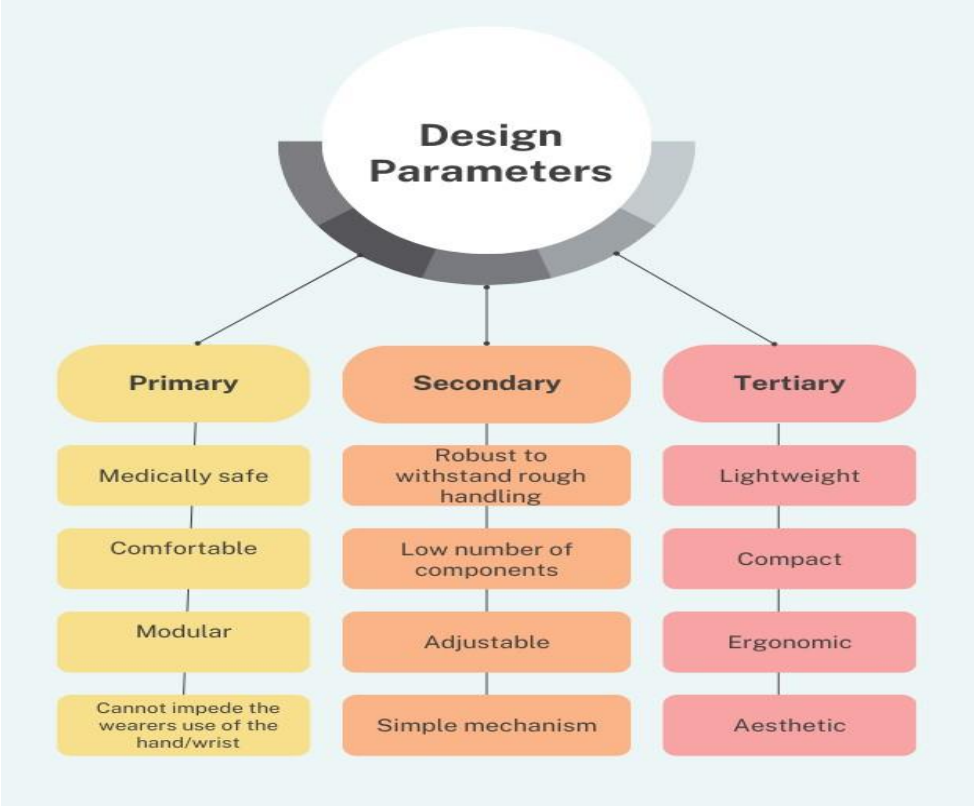

Figure 1. Design parameters of the new wrist splint

2.1. Conceptualization

Throughout the project, a 3-stage iterative design process was employed to develop the brace, encompassing the entire structure and each individual component. The primary areas of focus included the palm, back of hand, and thumb. At each stage, careful consideration was given to these key regions to ensure the brace offered optimal support and functionality. By iterating on the design, the team addressed any shortcomings or limitations, leading to overall performance improvements.

In designing the brace, particular attention was paid to the palm region to ensure adequate support and stability without compromising the wearer's dexterity or grip capabilities. Similarly, the back of the hand underwent similar scrutiny to strike a balance between structural integrity and flexibility. Emphasizing the importance of the thumb in hand movement, the design shown in figure 2 aimed to create a component that allowed for natural thumb motion while providing appropriate support to prevent further injury or strain.

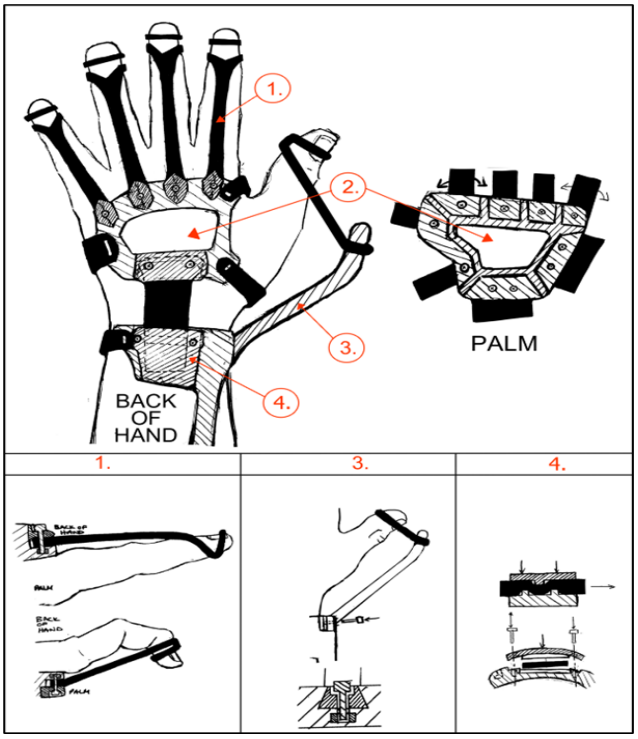

Figure 2. Final design concept of the wrist splint.

2.1.1. Measurement and dimensioning.

The hand with the identified point of interests (POIs) is depicted in figure 3. All measurements for these POIs were taken using the recommended wrist brace dimensions. The measurements of the hands were taken with a set of digital callipers.

Figure 3. Marked POIs on left hand, (a) back of hand, (b) palm, (c) side view.

2.1.2 Materials selection

For this design, a combination of hard and flexible materials is needed. TPU was chosen due to its flexibility and elastic properties, despite being more challenging to print and relatively costly. PLA, on the other hand, was selected for its biodegradability, affordability, and relatively high strength.

The RGU School of Engineering provided PRUSA PLA filament, including technical data necessary for finite element analysis (FEA). NinjaFLEX 85A TPU, known for its 65% elongation before yield and 660% elongation before break, was chosen for its elasticity. To join the components without using adhesives, M2.5x8mm Hex screws and M2.5x4x3.5 Brass threaded inserts were selected. The basic bill of materials for the wrist splint is presented in Table 1.

Table 1. Bill of materials for the new wrist splint

Material / Component	**Material Type**	**Amount (Kg or Pcs)**	**Quantity**	**Cost inc. Additional**	**Source Manufacturer**
PRUSA Polymers PLA	PLA	-	1	£ -	PRUSA polymers
NINJATEK NinjaFLEX 85A Midnight Black	TPU	1 KG	1	£76.90	NINJATEK
M2.5 x 4x 3.5 Threaded Inserts	Brass	100 Pcs	1	£4.16	Hitland
M2.5 x 8mm Hex Screw	Stainless Steel	30 Pcs	1	£5.99	A27 FAST
Total			£ 87.05		

2.1.3 Design and Manufacturing

The fabrication of the new wrist splint involved the use of two polymeric materials: polylactic acid (PRUSA PLA) and flexible polyurethane (NinjaFLEX 85A TPU). For PLA, the bed temperature and nozzle temperature were set at 250°C and 60°C, respectively (3). Considering the material properties, a print speed of 50 mm/s was selected for PLA, while a print speed of 20 mm/s was chosen for TPU. The specific slicer settings utilized in the fabrication process are provided in Table 2.

Table 2. Slicer settings

No.	Parameter/Printer	PRUSAMKIII	ENDER 3 Pro with Direct Drive Upgrade
1	Polymer type	PLA	TPU
2	Bed temperature	250°C	250°C
3	Nozzle temperature	60°	60
4	Support Angle	60°	FALSE
5	Support density	15%	FALSE
6	Cooling fan Speed	100%	100%
7	Retraction	On	Off
8	Print speed	50 mm/s	20 m/s
9	Wall thickness	1 mm	1 mm
10	Layer height	0.2 mm	0.1 mm

2.1.4 Analysis of resistance band

The deformed length (L) had to be established before the correct length (Lo) could be calculated for printing the digit and thumb resistance bands. The ANSYS Design modeller was used to recreate the resistance band model, and the resulting static structural analysis was subjected to considerable deformation. Parameters for the print length (Lo) and thickness (t), as well as the applied load and outcomes (figure 4), such as the location of a point of deformation and the maximum stress in the model, may be modified by reconstructing the model. Print length data ranged from 50 mm to 150 mm in 10 mm increments, thickness data ranged from 1 mm to 4 mm in 1 mm increments, and force data ranged from 0N to 30N in 5N increments, for a grand total of 263 models. Five parameters were obtained from a previous study by Tawk and Alici [18] using NINJATEK NinjaFLEX 85A and the MR model because TPU is a hyperelastic polymer. In order to input material properties into the ANSYS material database under the five-parameter MR model, the TPU material was tested in accordance with the testing standard ISO 37:2017, the results of which are displayed in Table 3.

	A	B	C	D
1	ID	Parameter Name	Value	Unit
2	Input Parameters			
3	RB-FDRB Static Analysis with Force, Thickness and Length Ranges (A1)			
4	P1	Lo	0.05	m
5	P2	t	0.001	m
6	P3	Force X Component	5	N
*	New input parameter	New name	New expression	
8	Output Parameters			
9	RB-FDRB Static Analysis with Force, Thickness and Length Ranges (A1)			
10	P4	Equivalent Stress Maximum	1.1442E+06	Pa
11	P5	Deformation Probe Maximum X Axis	0.0023439	m
*	New output parameter		New expression	
13	Charts			

Figure 4. ANSYS Hyper-elastic analysis input and output parameters.

Table 3. TPU hyper-elastic material model constants [18]

Hyper-Elastic Material Model	Material Constant	Value (Unit)
Five parameters Mooney-Rivlin	C10	-0.233 MPa
	C01	2.562 MPa
	C20	0.116 MPa
	C11	-0.561 MPa
	C02	0.9 MPa
	Incompressibility Parameter D1	0.0 MPa^{-1}

3. Results

The completed rehabilitation brace is shown in figure 5. When everything was finished and analysed the total weight was 220g.

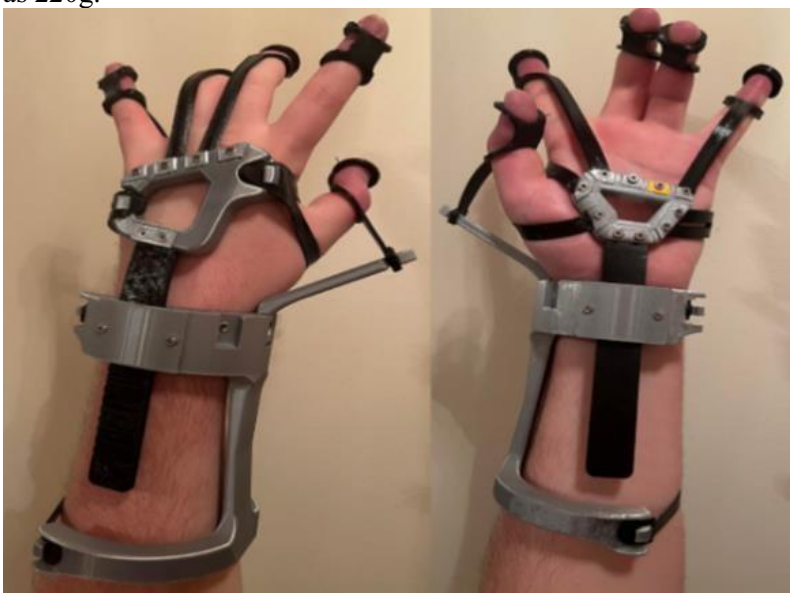

Figure 5. Final assembled burn rehabilitation brace worn in multiple views

3.1 Finite element analysis

The analysis models employed Default Meshing, with an illustration of the mesh presented in figure 6. The loading conditions, exemplified in figure 7, involved a fixed support at the fastener point and applied load parameters at the first digit hole. No external conditions were assumed or applied.

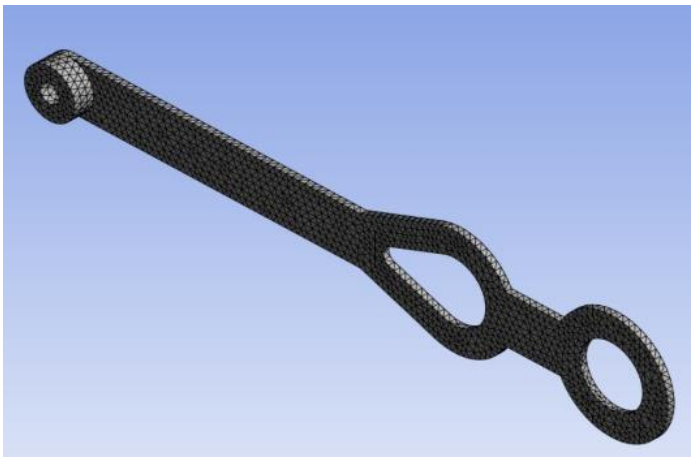

Figure 6. Resistance Band Analysis Mesh Example of t=1mm, Lo=50mm, F=5.

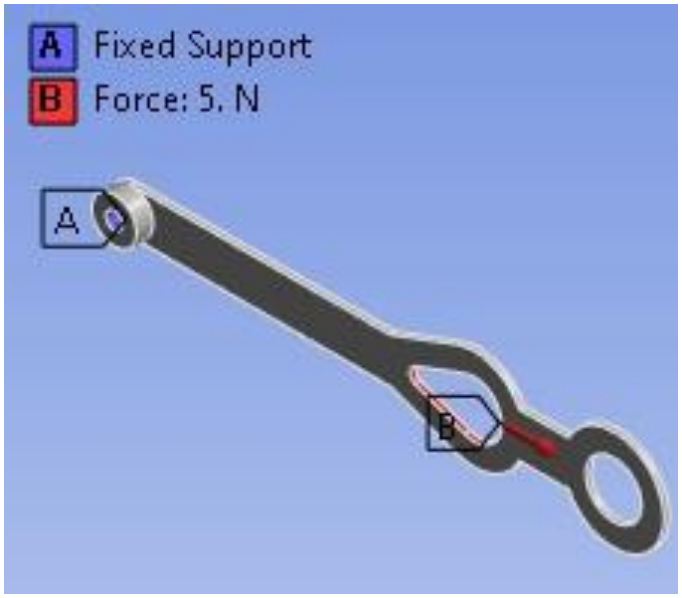

Figure 7. Resistance Band Analysis Loading Conditions Example of t=1mm, Lo=50mm, F=5.

The analysis and full results shown in figure 8 and processed in Microsoft Excel. Example of the results on an individual model are shown in figure 9 and 10.

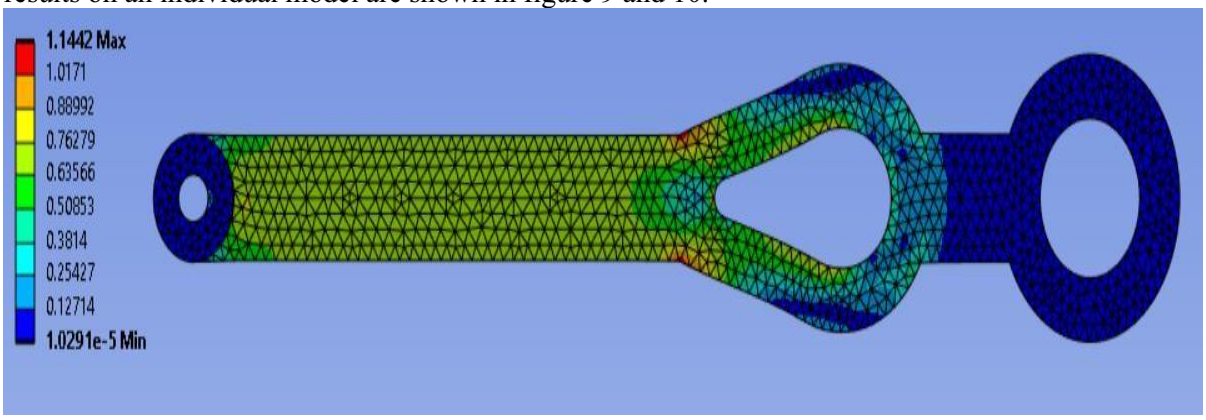

Figure 8. Resistance Band Analysis Stress Result (MPa) Example of t=1mm, Lo=50mm, F=5.

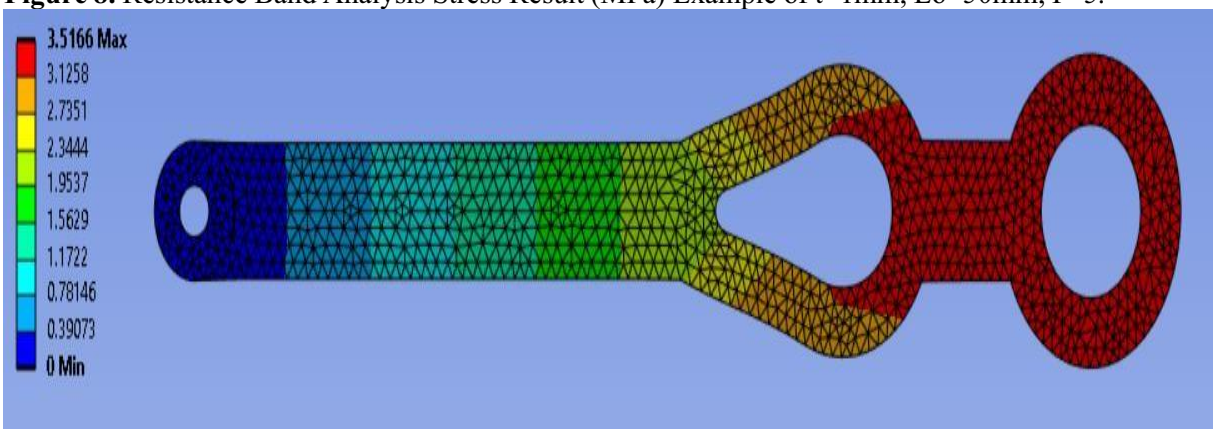

Figure 9. Resistance Band Analysis Deformation Result (mm) Example of t=1mm, Lo=50mm, F=5.

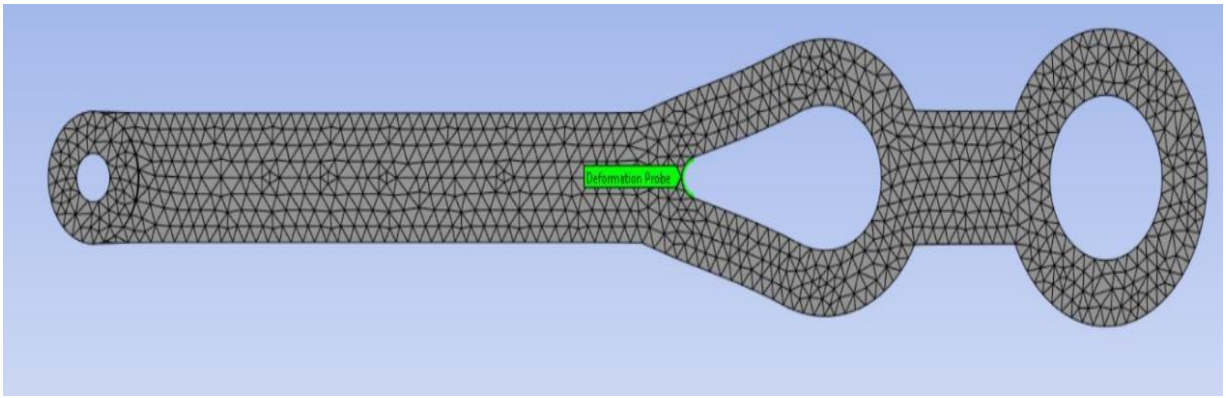

Figure 10. Resistance Band Analysis Deformation Probe Example of t=1mm, Lo=50mm, F=5.

Using the data collected, the force to material extension could be plotted for each analysis, where material extension (δ) is taken from the deformation probe and shown in equation (1).

$$\delta = \Delta L = L - L_o \quad (1)$$

In figure 11, the plot displays the material extension with varying original lengths but constant thickness, while figure 12 illustrates the material extension with varying thickness but a constant original length.

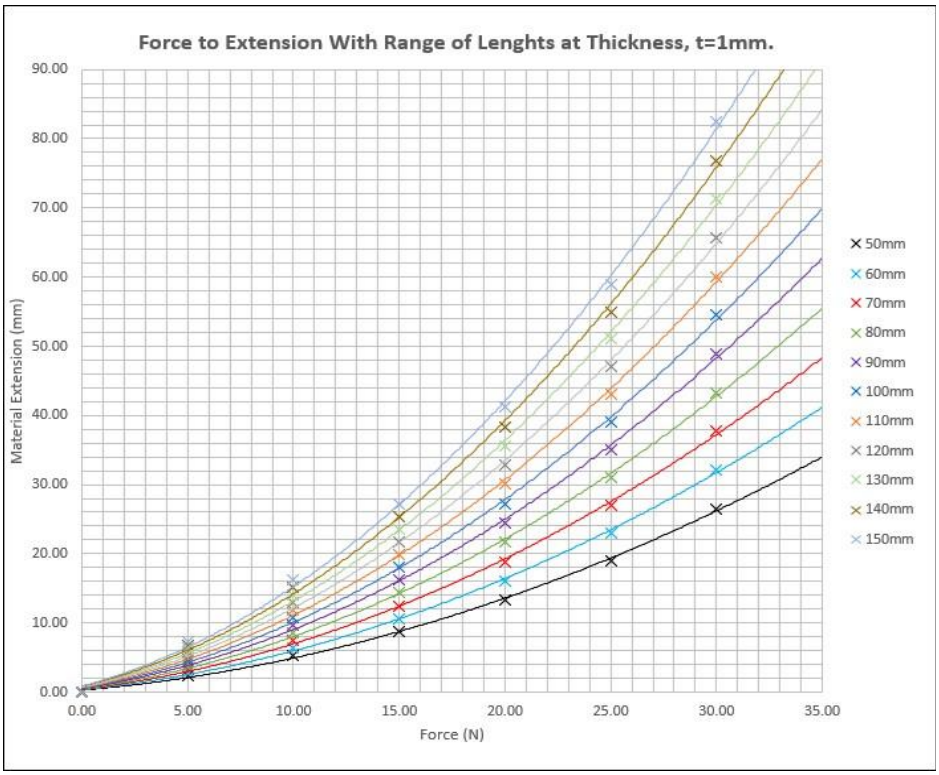

Figure 11. Plot of force to extension with range of lengths at thickness 1mm.

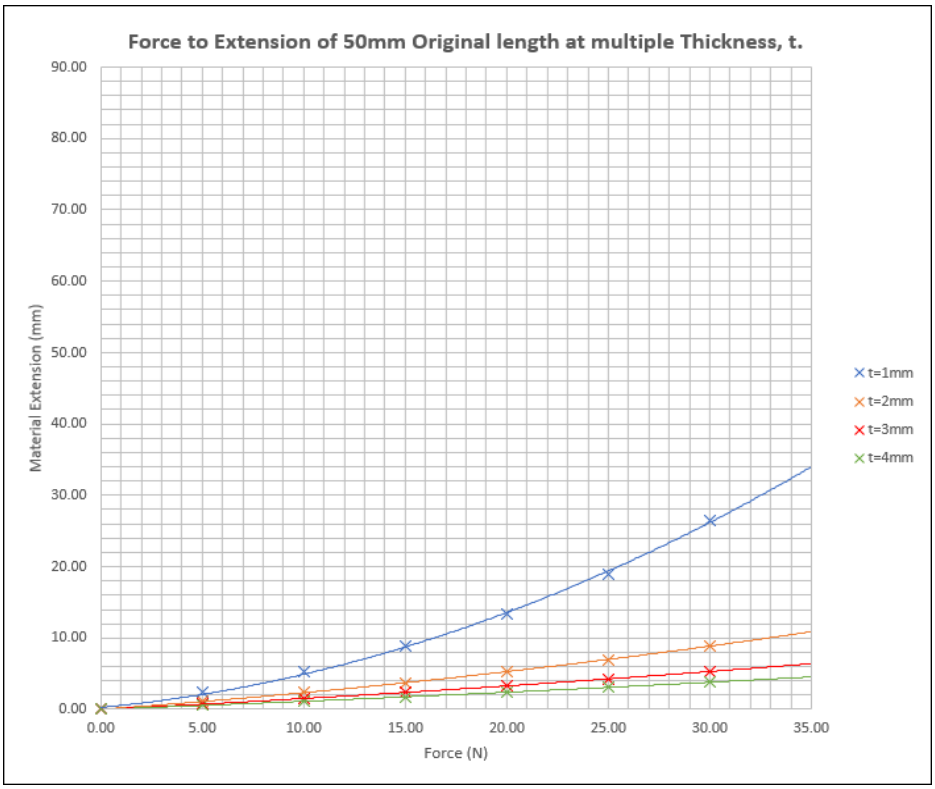

Figure 12. Plot of force to extension of 50 mm original length at multiple thickness, t.

These results can be compared to linear analysis calculations using the material properties provided by technical data sheet.

Table 4. Material Properties of NinjaFlex 85A

MATERIAL PROPERTIES NINJAFLEX TPU 85A (midnight black)		
Property	Value	Unit
Youngs Modulus	12	Mpa
Poisson Ratio	0.48	-
Density	1190	kg/m^3
Ultimate Tensile	26	MPa
Yield Tensile	4	MPa
Tield Elongation	65	%
Break Elongation	660	%
Hardness	85	Shore A
Max Safe Stress	13	MPa

This assumes that the deformation within the elastic stage is linear. The following equations were used to compute Lo and A.

$$L_0 = \frac{L}{\left(\frac{F}{EA}\right)+1} \quad (2)$$

Where,

$$A = Bt \quad (3)$$

B, is the width of the resistance band of 8 mm and t is the thickness. Using Excel, the linear calculation can be determined over the same range of parameters as the ANSYS Static Structural Analysis. An example of the calculation vs. ANSYS Analysis can be seen in table 5.

Table 5. ANSYS analysis versus linear calculation example table of results.

Sim Vs Linear Calculation 1			
Lo - 50mm t = 1			
A= 0.000008 m^2			
		δ (mm)	
Lo (mm)	F (N)	Sim	Calc
50	0	0	0
50	5	2.34387	2.604167
50	10	5.224004	5.208333
50	15	8.801136	7.8125
50	20	13.28768	10.41667
50	25	19.00738	13.02083
50	30	26.511	15.625

Using the results obtained from the ANSYS Analysis versus linear calculation, the following plots of ANSYS MR analysis against linear deformation can be created and shown in figure 13, figure 14 and figure 15.

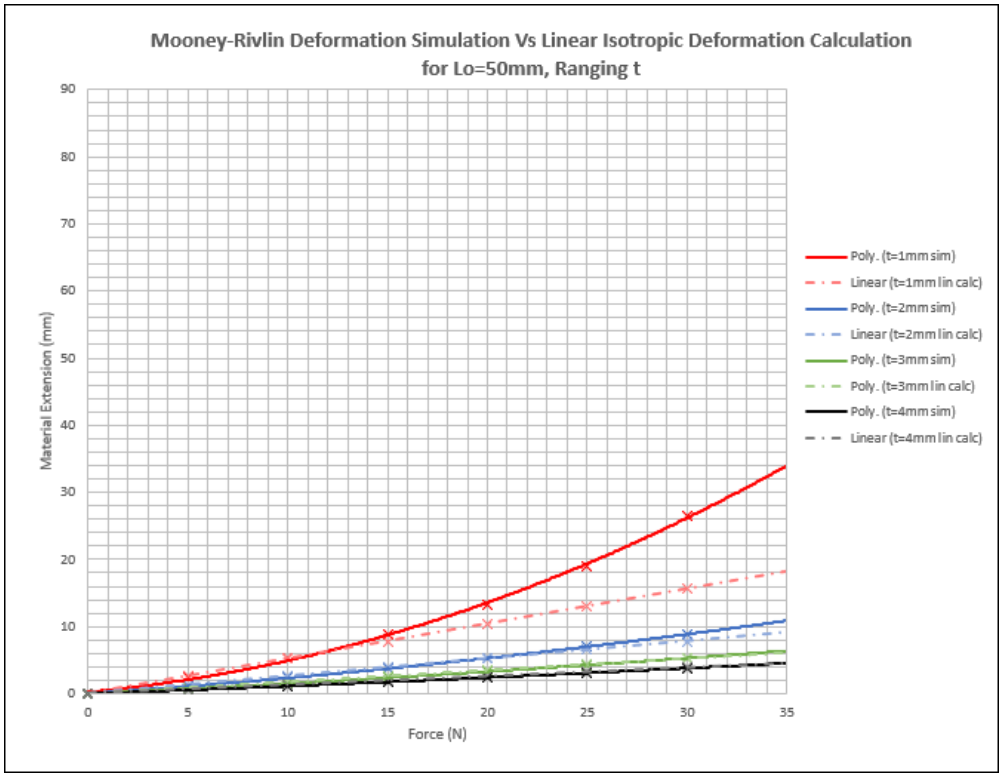

Figure 13. Plot ANSYS MR analysis Vs. linear deformation calculation for Lo=50mm, ranging t.

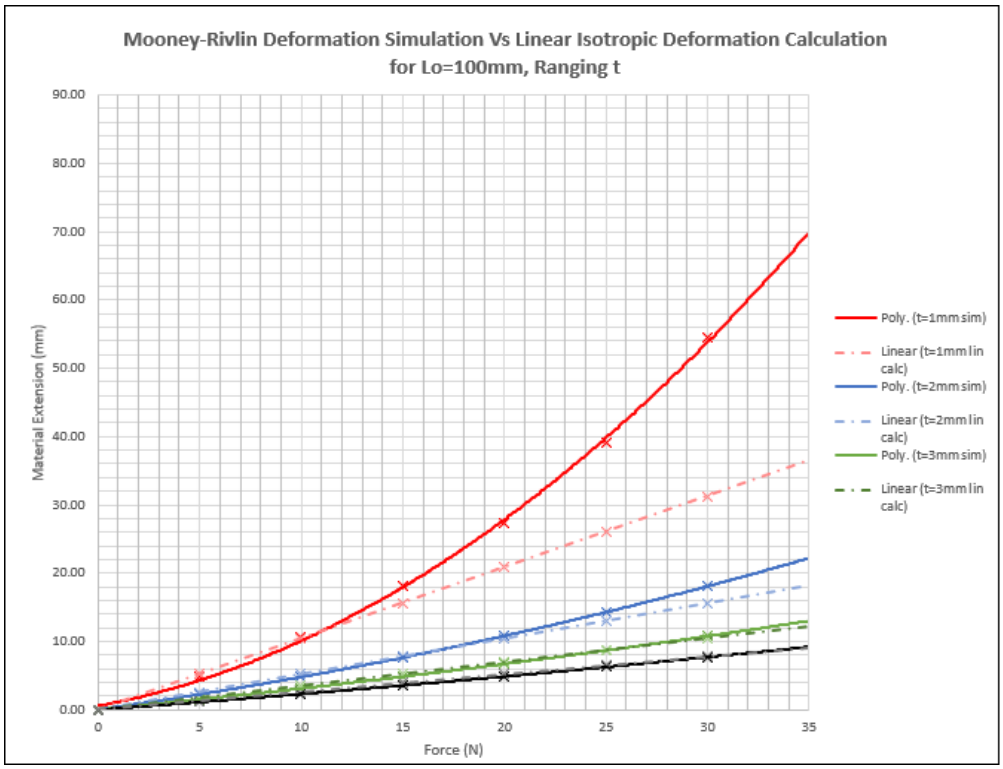

Figure 14. Plot ANSYS MR analysis Vs. linear deformation calculation for Lo=100mm, ranging t.

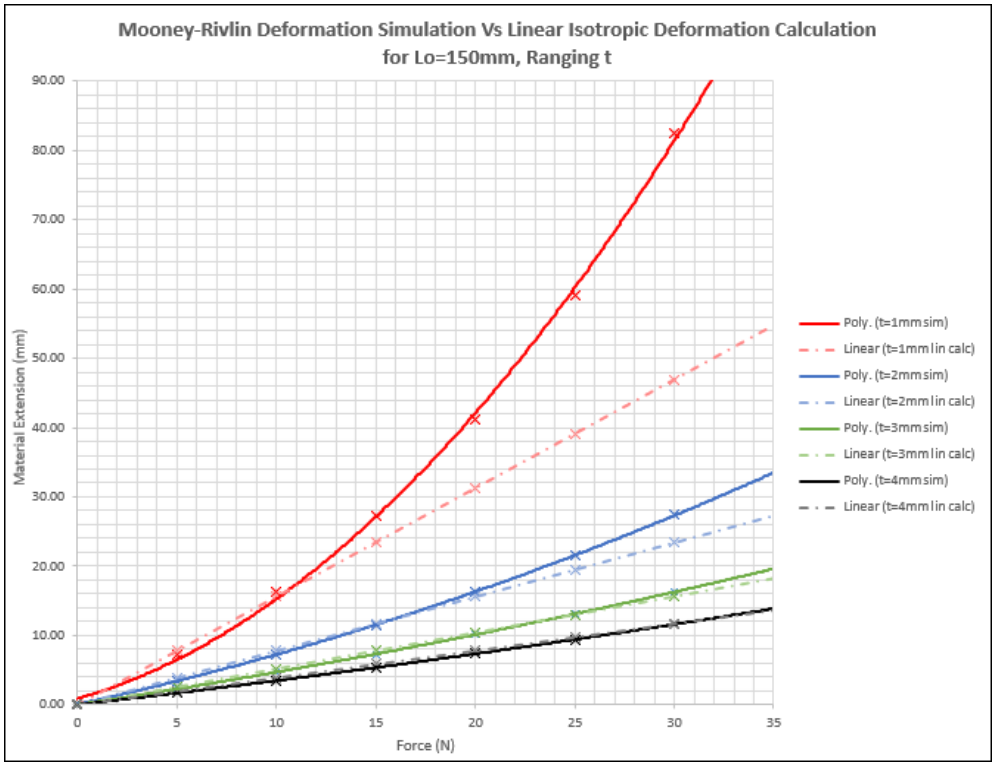

Figure 15. Plot ANSYS MR analysis Vs. linear deformation calculation for Lo=150mm, ranging t.

The results show that the ANSYS Analysis remains almost linear between 0N and 20N for thicknesses between 2 mm and 4 mm with variable Lo, but deviates after that. The linear computation begins to deviate from the 1mm thickness example at 5N. Therefore, the linear relationship described by equation 2 may be utilised to accurately anticipate the printing length of the digit and thumb resistance bands for thicknesses between 2 mm and 4 mm and loading between 0N and 20N. However, equation 2 is not appropriate for forecasting the printing length of the resistance bands at a thickness of 1 mm. When comparing the tensions across different thicknesses, it is clear that the 1mm thickness is under the most pressure. Table 6 provides an illustration of this point, showing that the maximum stress in the 1 mm thickness is greater than twice that in the 2 mm thickness for all loading conditions. This means that 1mm thickness is more likely to experience a catastrophic failure than other thicknesses.

Table 6. ANSYS analysis maximum stress comparison, 1 mm vs. 2 mm thickness.

t = 1mm			t = 2mm		
lo11 (mm)			lo11 (mm)		
150			150		
F (N)	δ (mm)	σ (Mpa)	F (N)	δ (mm)	σ (Mpa)
0.00	0.00	0.00	0.00	0.00	0.00
5.00	7.28	1.20	5.00	3.45	0.61
10.00	16.19	2.34	10.00	7.30	1.18
15.00	27.26	3.51	15.00	11.54	1.74
20.00	41.18	4.81	20.00	16.25	2.29
25.00	59.00	6.34	25.00	21.50	2.85
30.00	82.44	8.21	30.00	27.36	3.43

4. Discussion

The static FEA on each component does not account for layer separation, material flaws, or warping in the printed component, which can dramatically reduce its strength, as seen by critical failures between layer lines. However, static analysis shows how stresses affect the model and where critical failure is probable, identifying regions where more material can strengthen components. FEA shows stress distribution and model deformation, which computations cannot anticipate.

Topology optimisation on the wrist brace base component resulted in a 13g mass shift between the optimised product and the final model of iteration 3. FEA analysis of TPU resistance bands, which did not account for printing defects, yielded results similar to linear calculations for loading in the range of 0N-20N with band thicknesses of 2mm-4mm, indicating theoretical accuracy.

To compare resistance bands and PLA components with FEA analysis, further experimental data and testing are needed. To better simulate material deformation, use different hyper-elastic models.

Mesh convergence improves model mesh without increasing simulation run time, improving FEA accuracy. Broadening component model loading permits observation of their behaviour under lower and higher loading levels than required. FEA can improve by considering model effect and modelling a larger range of temperatures to mimic external environmental conditions.

Test prints, support material, unsuccessful prints, and final prints utilised 0.616kg of PLA. Test and unsuccessful prints used 0.307kg, support material 0.115kg, and finalised prints 0.194kg, wasting

0.422kg of PLA. TPU, including test and final prints, was 0.05kg, with 0.019kg wasted. Each unit has 23 brass inserts and 21 M2.5x8 screws, weighing 0.225kg.
The project's total material cost is £25.63, with £12.86 of waste, based on the official PRUSA company's quote of £26.99 for a 1kg PLA spool. £12.77 per unit excludes FDM 3D printers and labour.

5. Conclusion

The successful creation of a wrist splint for burn patients was achieved through the utilization of 3D printing methodologies in the design and production process. This report's iterative design method produced the burn rehabilitation wrist and hand brace. When measured, the resistance bands push against the digits. While exerting stress to the hand and digits, the wrist resistance bands and bases secure the hand. The clamp secures the wrist resistance band while allowing hand movement. The brace fits well and is comfortable except for the resistance band digit attachment. The unit weighed 0.23kg and used 0.67kg of material. No experimental data on burn patients was collected, but similar methods for stroke victims have demonstrated beneficial effects. FEA static structural analysis of PLA components shows that the design can survive applied forces with large safety margins, but printing defects were not considered, causing certain test prints to fail. TPU resistance bands can endure applied stresses before plastic deformation, according to FEA, although printing errors were not considered. However, FEA studies showed linear deformation for stresses 0-20N and thicknesses 2-4mm, allowing linear calculations to reliably forecast printing length. Topology optimisation reduced wrist brace base mass by 13g. The project cost £87.05. Unused material cost £61.42. Waste cost £12.86, and each brace cost £12.77, omitting energy and labour.

References

[1] Jeschke M G, van Baar M E, Choudhry M A, Chung K K, Gibran N S and Logsetty S 2020 Burn injury *Nat Rev Dis Primers* **6**
[2] Yang Y S, Emzain Z F and Huang S C 2021 Biomechanical Evaluation of Dynamic Splint Based on Pulley Rotation Design for Management of Hand Spasticity *IEEE Transactions on Neural Systems and Rehabilitation Engineering* **29** 683–9
[3] Momeni M 2019 *Effectiveness of incorporating occupational therapy in rehabilitation of hand burn patients*
[4] Ghalayini G, O'Brien L and Bourke-Taylor H M 2019 Recovery in the first six months after hand and upper limb burns: A prospective cohort study *Aust Occup Ther J* **66** 201–9
[5] Dargan D, Himmi G, Anwar U, Jivan S and Muthayya P 2022 A comparison of the epidemiology of isolated and non-isolated hand burns *Burns*
[6] Oosterwijk A M, Mouton L J, Schouten H, Disseldorp L M, van der Schans C P and Nieuwenhuis M K 2017 Prevalence of scar contractures after burn: A systematic review *Burns* **43** 41–9
[7] Schneider J C, Qu H D, Lowry J, Walker J, Vitale E and Zona M 2012 Efficacy of inpatient burn rehabilitation: A prospective pilot study examining range of motion, hand function and balance *Burns* **38** 164–71
[8] Schouten H J, Nieuwenhuis M K, van Baar M E, van der Schans C P, Niemeijer A S and van Zuijlen P P M 2019 The prevalence and development of burn scar contractures: A prospective multicenter cohort study *Burns* **45** 783–90
[9] Mc Kittrick A, Gustafsson L, Hodson T and Di Tommaso A 2023 Exploration of individuals perspectives of recovery following severe hand burn injuries *Burns* **49** 467–75
[10] Kara S, Seyhan N and Öksüz S 2023 Effectiveness of early rehabilitation in hand burns *Ulus Travma Acil Cerrahi Derg* **29** 691–7

[11] Oosterwijk A M, Mouton L J, Schouten H, Disseldorp L M, van der Schans C P and Nieuwenhuis M K 2017 Prevalence of scar contractures after burn: A systematic review *Burns* **43** 41–9
[12] Schouten H J, Nieuwenhuis M K and Van Zuijlen P P M 2012 A review on static splinting therapy to prevent burn scar contracture: Do clinical and experimental data warrant its clinical application? *Burns* **38** 19–25
[13] Muhamad W, Saharudin W M, Abd M S, Wahid K A, Saniman M N F and Reshid M 2020 *Nozzle Design for fused deposition modelling 3D Printing of carbon fibre reinforced polymer composite component using simulation method* vol 17
[14] Ali Nahran S, Saharudin M S, Mohd Jani J and Wan Muhammad W M 2022 The Degradation of Mechanical Properties Caused by Acetone Chemical Treatment on 3D-Printed PLA-Carbon Fibre Composites *Advanced Structured Materials* vol 167 (Springer Science and Business Media Deutschland GmbH) pp 209–16
[15] Kechagias J, Kitsakis K, Zacharias A, Theocharis K, Aslani K E, Petousis M, Fountas N A and Vaxevadnidis N M 2021 Direct 3D Printing of a hand splint using Reverse Engineering *IOP Conference Series: Materials Science and Engineering* vol 1037 (IOP Publishing Ltd)
[16] Mian S H, Umer U, Moiduddin K and Alkhalefah H 2023 Finite Element Analysis of Upper Limb Splint Designs and Materials for 3D Printing *Polymers (Basel)* **15** 2993
[17] Mohamad Nor Azli M S, Mohd Radzi M F, Che Nasir N A and Saharudin M S 2023 Design of a Pre-crack Device for Environmental Stress Cracking (ESC) Studies *Advanced Structured Materials* vol 173 (Springer Science and Business Media Deutschland GmbH) pp 163–74
[18] Tawk C and Alici G 2020 Finite element modeling in the design process of 3D printed pneumatic soft actuators and sensors *Robotics* **9**